ELSEVIER

Journal of Electroanalytical Chemistry 461 (1999) 80–89

JOURNAL OF ELECTROANALYTICAL CHEMISTRY

Structural specificity of the kinetics of the hydrogen evolution reaction on the low-index surfaces of Pt single-crystal electrodes in 0.5 M dm^{-3} NaOH[1]

J.H. Barber [a], B.E. Conway [b,*]

[a] *E-CELL Corp., 52 Royal Road, Guelph, Ontario N1H 1G3, Canada*
[b] *University of Ottawa, Department of Chemistry, Ottawa, Ontario K1N 6N5, Canada*

Received 24 November 1997; received in revised form 16 April 1998; accepted 16 April 1998

Abstract

The kinetics of the underpotential deposition (upd) of H and the hydrogen evolution reaction (her) have been found to be extremely sensitive to the surface geometry of Pt single-crystal surfaces. The order of electrocatalytic activity at the low-index planes was found in our previous studies to be (100) < (111) < (110). The study of the kinetics of the her at Pt(hkl) electrodes in 0.5 M H_2SO_4 is found to be complicated by the influence of H_2 diffusion away from the surface. However, increase of the pH decreases the kinetic facility of the hydrogen electrode reaction, i.e. abstraction of H to form H_2 is more difficult from H_2O than from H_3O^+; at such lower rates, diffusive effects can be totally eliminated by electrode rotation. In the present paper we show that in 0.5 M NaOH the order of reactivity is identical with that found in acidic media, viz. (100) < (111) < (110). The slower rates arising in alkaline media allow a larger potential range to be probed and, unlike the situation in acid, quantitative rate information for each of the Volmer, Heyrovsky and Tafel steps of the her was obtained by using electrochemical impedance spectroscopy (EIS) and steady-state dc methods. As well as rate information, the charge, q_1, corresponding to maximum fractional coverage by the overpotentially deposited H species (opd H), can be obtained and will be discussed in terms of the results previously found in acid, related to surface geometry and coverage by upd H. The results of the present work will also be compared with those of other recent studies conducted in alkaline media.

Keywords: Hydrogen evolution reaction; Structural specificity; Pt single crystal electrodes

1. Introduction

Recent reports from this laboratory have shown that the kinetics of both upd [1] and opd of H [2] in the her, and the latter's overall rates, are dependent on the surface lattice geometry at Pt single-crystal electrodes, in 0.5 M H_2SO_4 [2]. In previously published work [3–6] concerning this subject it was surprising that the her kinetics were found to be independent of the surface geometry in spite of the well known [7] large range in the values of the exchange current-density (j_0) of the her for a variety of metals and the related [8] respective work functions of the cathodic substrate metals. Electrocatalysis, at metals, like catalysis, has been found to be highly specific to the nature of the electrode-metal substrate [7,8], and to the geometry and electronic properties of its active surface [9]. Such behaviour is clearly manifested in the kinetics of small molecule oxidation processes at various anode materials as extensively studied by Vielstich et al. [10]. From such studies, important applications in fuel-cell development [11] have arisen. More recently, such specificities in electrocatalysis and electrosorption have been clearly demonstrated at single-crystal surfaces, e.g. for upd of H and

* Corresponding author. Tel.: +1 613 5625481; e-mail: jbarber@glegg.com

[1] Dedicated to Professor W. Vielstich on the occasion of his 75th birthday.

0022-0728/99/$ - see front matter
PII S0022-0728(98)00161-2

the H_2 evolution reaction (her) at the Pt principal index and other stepped-surface planes [1,2]. In Barber et al. [2] it was shown that the surface-geometry dependence of the her kinetics in 0.5 M H_2SO_4 at Pt electrodes is obscured by a rate-influencing H_2 diffusion process. To be able to study electrochemical reactions which have extremely fast electron transfer rates, and which are consequently influenced by reactant or product diffusion, complementary time or frequency dependent methods must be used. Jahn and Vielstich [12], studying the Fe^{2+}/Fe^{3+} couple, provided one of the first examples of how rotation-rate studies could be used to determine kinetic parameters. Similar rotation-rate methods in combination with EIS measurements were employed in our previous work [2] which allowed the separation of the kinetic and diffusive influences of the her at Pt(hkl) electrodes in 0.5 M H_2SO_4, leading to a quantitative analysis of the electrode kinetics as a function of Pt surface geometry. The results in Barber et al. [2] indicate that the reactivity of the low-index planes follows the order (100) < (111) < (110) in 0.5 M H_2SO_4; in fact the rates of the her processes at the (110) and (poly) surfaces were so rapid that the her kinetics were dominated, and thus obscured, by the slower H_2 diffusion rate. The rates for H_2 evolution are, however, significantly slower in basic solutions [13] due to the H atom being abstracted from H_2O instead of the hydronium ion H_3O^+ in acid media. In order to compare the her rates at the (110) and (poly) surfaces in acidic and alkaline solutions, studies were undertaken on all the low index planes in 0.5 M NaOH. Similar to what was found in acidic media, in 0.5 M NaOH substantial differences in the her kinetics arise at a series of Pt single-crystal surface structures and, as well, differences in the absolute (potential dependent) coverages of opd H are also observed.

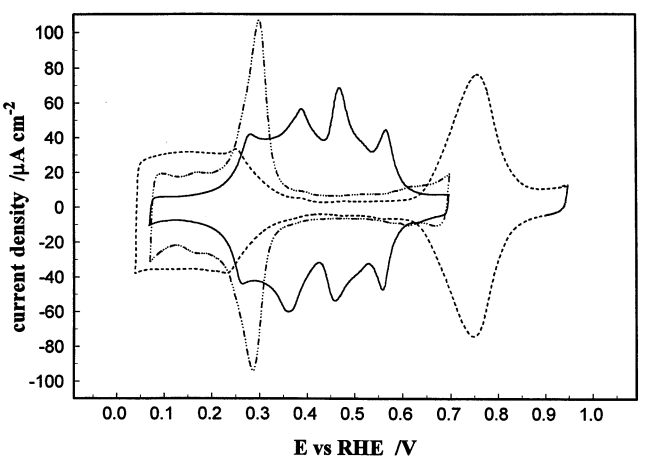

Fig. 1. Cyclic voltammograms of the three low-index planes of Pt in 0.5 M NaOH; scan rate 50 mV s^{-1};—(100), –···–(110), and ---(111).

2. Experimental

The Pt single-crystal electrodes were prepared by the procedure given in our previous paper [2], based on details given in earlier works by Clavilier et al. [14]. The cyclic voltammograms for the upd of H in 0.5 M NaOH for the three low-index planes were first recorded in order to verify solution cleanliness and electrode structure and these CVs are shown in Fig. 1; their characteristic profiles are seen to be similar to those reported respectively in the literature [15]. Solutions of electrolytic NaOH were prepared from either BDH Aristar NaOH pellets (minimum assay 98.0%, $Na_2CO_3 \approx 2\%$) or Alfa AESAR NaOH pellets (minimum assay 99.996%) dissolved in millipore 18.2 MΩ water. These two solutions provided identical results for the CVs, steady-state dc and EIS measurements.

The single-crystal electrodes were mounted on to a Pine AFASR 701 analytical rotator assembly via a Teflon holder. The her measurements were acquired at rotation rates of 3000 rpm and an increase to higher rotation rates, up to 4000 rpm, produced unchanged EIS and steady-state dc results. Importantly, no diffusive processes were detectable in the ac impedance spectra at 3000 rpm, e.g. the distorted semicircle in the complex-plane impedance plot characteristic of diffusion through finite-layer thickness, was not observed.

Cyclic voltammograms were recorded using a Hokuto-Denko 501 potentiostat controlled by a EG&G PAR 175 function generator. The current and voltage were recorded on a Nicolet 310 digital oscilloscope followed by processing on an IBM compatible computer. EIS data were recorded using a Solartron 1286 electrochemical interface in conjunction with a Solartron 1255 frequency response analyser. The EIS data were fitted using the software LEVM 6.0, which can perform complex nonlinear least squares (CNLS) analysis. This programme was modified for interpretation of the results according to the ac impedance model for the her derived in Harrington and Conway [16], given below as Eqs. (6) and (7). Once modified, the LEVM program was compiled and operated using an IBM AIX UNIX system.

For some of the single-crystal surfaces it was found that the steady-state cathodic current-density was unsteady after initial cathodic polarization and that a certain time was required before the EIS measurements could be satisfactorily recorded. The change in the current-density after cathodic polarization was dependent on both the polarization potential and the surface under study. At the (111) and (100) surfaces at low overpotentials, the current decreased slightly, by ca. $\leq 10\%$ for the (111) and 10–20% for the (100). For the (100) at higher overpotentials and the (110) and polycrystalline surfaces the current-density increased initially anywhere from 10 to 600% depending on the

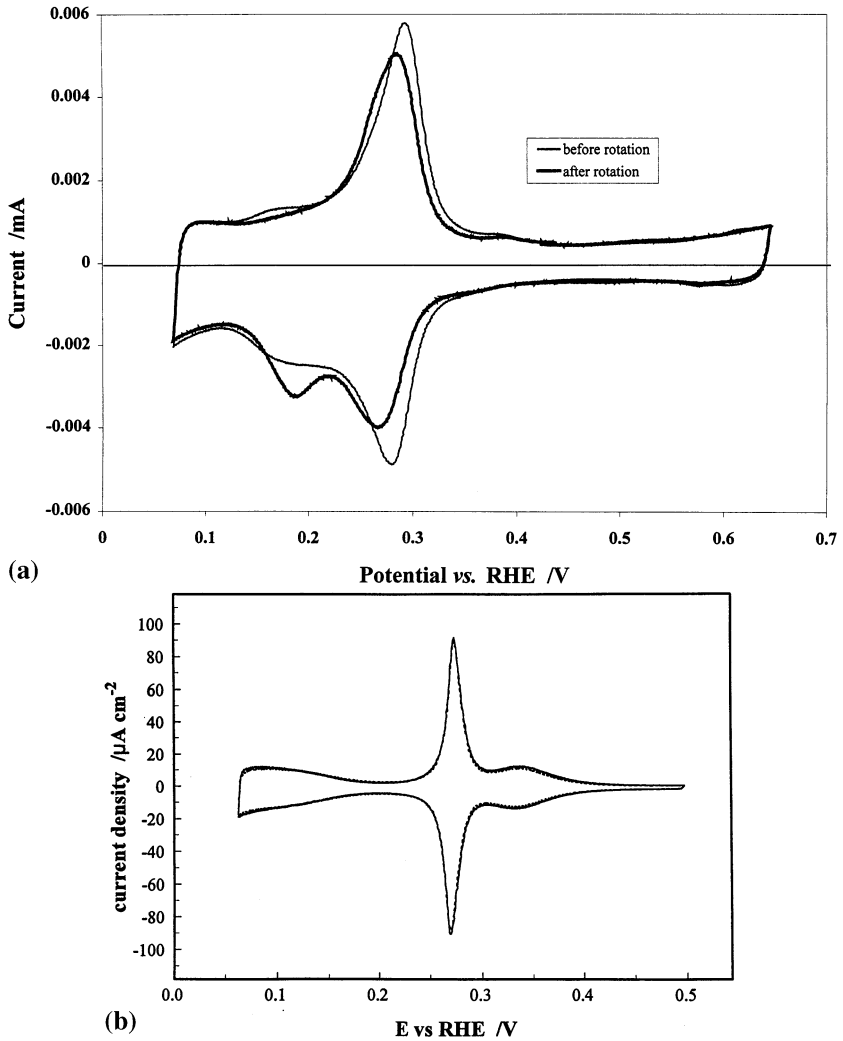

Fig. 2. (a) Cyclic voltammograms for the H upd region at a Pt(110) surface in 0.5 M (—) before and (—) after cycling for 2 min at a rotation rate of 2000 rpm. Potential scan rate 50 mV s^{-1}, 23°C. (b) Cyclic voltammograms for the H upd region at a Pt(511) surface before and after an EIS measurement (approximately 2 min) in the her region and 5 min in the upd H region, for removal of H_2. Potential scan rate 20 mV s^{-1}.

potential and the surface being studied. After this increase, the current remained constant for the duration of the frequency scan. This behaviour suggests that the effect at the (111) and (100) planes is not simply due to adventitious poisoning. In fact, throughout the work, the 'high-purity' techniques developed in earlier years by us and others were rigorously applied. However, it is well known that very high purity of aqueous NaOH solutions is more difficult to attain than for acid solutions.

In order to examine this matter further, the effect of rotation on the H upd voltammogram for the Pt(110) surface, as an example, was recorded as shown in Fig. 2a before and after 2 min of cycling at an electrode rotation rate of 2000 rpm. From these plots it is seen that small but significant changes in the form of the voltammogram arise; however, the H upd charge, which is a sensitive indicator of the presence of adsorbed impurities, is only a little diminished, by less than 4%. A related voltammetry experiment at a Pt(511) surface performed in 0.5 M NaOH, conducted before and after the extended period of time required for removal of H_2 after cathodic polarization in the opd region, showed (Fig. 2(b)) virtually no change in the voltammogram. This provides a good confirmation of the absence of significant poisoning effects.

Complementary to the study of rotation on the cyclic voltammograms (Fig. 2(a, b)), an electrode rotation experiment was conducted on the her kinetics at a Pt(poly) electrode. Fig. 3 shows the effect of rotation at 500 and 3000 rpm on the Tafel relationship for the her at the cathodically polarized electrode. Currents over the whole overpotential range are seen to be increased by electrode rotation rather than being decreased which would have been the case had significant poisoning effects been operative. Thus, such effects, when present, are usually enhanced by electrode rotation due to facilitated transport of the imp species to the electrode interface.

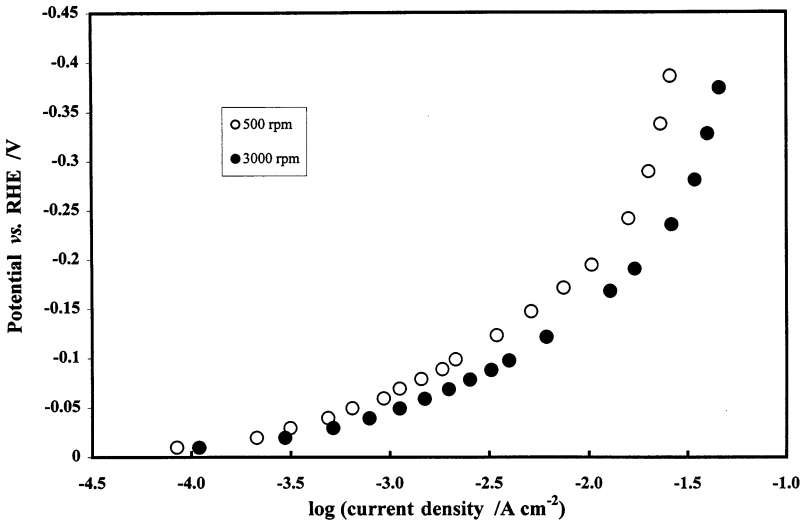

Fig. 3. The effect of electrode rotation at 500 and 3000 rpm on the Tafel relation for the her in 0.5 M NaOH solution at a Pt(poly) electrode.

3. Kinetics and impedance behaviour

The her reaction mechanism in alkaline solutions follows the well known three-step process of electrochemical hydrogen adsorption: the Volmer step:

$$H_2O + e^- + M \underset{k_{-1}}{\overset{k_1}{\rightleftarrows}} M^-H_{ads} + OH^- \quad \text{(I)}$$

followed by either the electrochemical H desorption, Heyrovsky step:

$$M - H_{ads} + H_2O + e^- \underset{k_{-2}}{\overset{k_2}{\rightleftarrows}} H_{2(g)} + OH^- \quad \text{(II)}$$

or the H + H combination reaction, Tafel step:

$$2M - H_{ads} \underset{k_{-3}}{\overset{k_3}{\rightleftarrows}} H_2 \quad \text{(III)}$$

Assuming Butler–Volmer electrode kinetics and Langmuir adsorption of opd H, and writing F/RT as f, the rate equations for steps I, II and III are expressed as [2]:

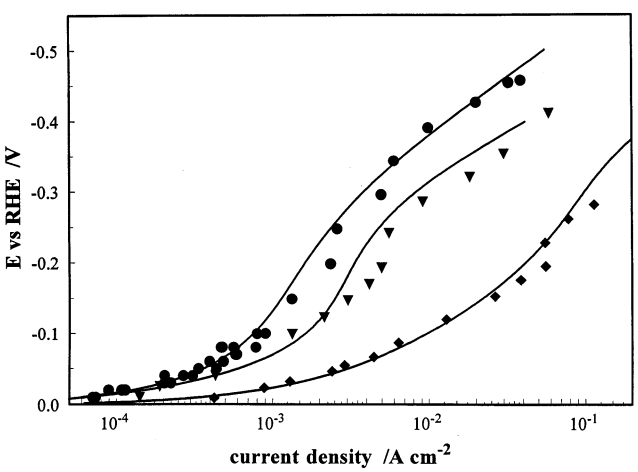

Fig. 4. Tafel plots for the her at the three low-index planes of Pt. Each point corresponds to one EIS measurement. Rotation rate 3000 rpm; best fit line calculated from the rate constants in Table 1; ● (100), ▼ (111) and ◆ (110).

$$\upsilon_1 = k_1(1-\theta_H)\exp(\beta\eta f) - k_{-1}\theta_H \exp((1-\beta)\eta f) \quad (1)$$

$$\upsilon_2 = k_2(1-\theta_H)\exp(\beta\eta f) - k_{-2}\theta_H \exp((1-\beta)\eta f) \quad (2)$$

and

$$\upsilon_3 = k_3\theta_H^2 - k_{-3}(1-\theta_H)^2 \quad (3)$$

The steady-state current-density is written as:

$$j_{tot} = Fr_0 = F(\upsilon_1 + \upsilon_2) \quad (4)$$

with r_0 representing the flux of electrons transferred at the electrode surface. The fractional opd H coverage (θ_H) (i.e. the coverage additional to the upd coverage already present at $\eta = 0$) is evaluated using the steady-state condition:

$$\frac{q_1}{F}\frac{d\theta_H}{dt} = 0 = r_1 = \upsilon_1 - \upsilon_2 - 2\upsilon_3 \quad (5)$$

with r_1 representing the net rate of production of the adsorbed H intermediate.

Following the procedure of Harrington and Conway [16], the faradaic admittance can be derived by expanding r_0 and r_1 in two Taylor series limited to the first-order terms; the two resulting equations are then solved for $\Delta j/\Delta E$, giving:

$$Y_f = A + \frac{B}{(i\omega + C)} \quad (6)$$

with $A = -F(\partial r_0/\partial E)_\theta$, $B = (F^2/q_1)(\partial r_0/\partial\theta_H)_E(\partial r_1/\partial E)_\theta$, $C = -(F/q)(\partial r_1/\partial\theta_H)_E$ and q_1 representing the charge required for creating full fractional coverage, $\theta_H = 1$, by opd H. Including the solution resistance (R_s) and the double-layer capacitance, the total impedance is given as:

$$Z_{tot} = R_s + (Y_f + i\omega C_{dl})^{-1} \quad (7)$$

Table 1

Orientation	$10^8\ k_1$/mol cm^{-2} s^{-1}	$10^7\ k_{-1}$/mol cm^{-2} s^{-1}	$10^{10}\ k_2$/mol cm^{-2} s^{-1}	$10^7\ k_3$/mol cm^{-2} s^{-1}	$10^4\ q_1$(opd) /C cm^{-2}
(100)	0.66 ± 0.07	0.195 ± 0.03	1.5 ± 0.2	0.07 ± 0.02	0.3**
(111)	1.3 ± 0.2	7.0 ± 1	0.86 ± 0.1	0.15 ± 0.02	0.6 ± 0.2
(110)	2.5 ± 0.2	2.9 ± 0.6	4.3 ± 8	4.9 ± 2	1.1 ± 0.2
(poly)*	1.0	3.0	2.0	2.8	0.7

* Result from Harrington and Conway [16]. ** Estimated value based on results from Barber et al. [2].

It was found in the course of the data analysis that a much better fit of the EIS data could be achieved when the double-layer capacitance element was replaced with a constant-phase element (cpe) its admittance is expressed as:

$$Y_{\mathrm{cpe}} = (\mathrm{i}\omega)^{\phi} T \tag{8}$$

Although, the requirement for use of the cpe is usually associated with porosity of the working electrode [17], this cannot be the situation here; it was thought this may be related to current distribution in the meniscus, but the effect was also seen for an immersed polycrystalline electrode. The results from the analysis showed that the phase-angle was close to 90°; therefore whatever the process is its effect is small. It is unlikely also that the depression of the high frequency semicircle could have been due to the deactivation processes which arose to a limited extent, as was discussed in the experimental section; the reason is that the cpe was required either when the steady-state current-density was slightly decreasing (as for Pt(100) at low η and Pt(111) at all η) or slightly increasing (as for Pt(110) at all η and (100) at high η).

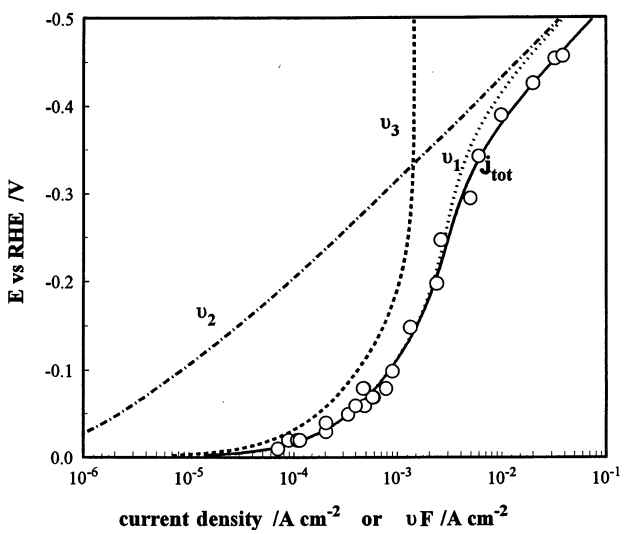

Fig. 5. A Tafel plot for the (100) surface as in Fig. 4, including the contributions of the three steps in units of current-density (A cm^{-2}). Symbols indicate data: ○ (j_{tot}), ··· Fv_1, -·-Fv_2, and --- Fv_3.

4. Results and discussion

In Fig. 4 the steady-state current-density versus potential relationships are compared in Tafel plots. Each current-density/potential point in Fig. 4 corresponds to one ac impedance frequency scan, the results from this analysis being shown later. The lines in Fig. 4 are calculated from the values of the derived rate constants listed in Table 1, which were evaluated by means of simultaneous fitting of the current-density versus potential and the A ($1/R_{\mathrm{ct}}$) (see definition below Eq. (6)) versus potential relationships. The salient features of Fig. 4 are:

1. The order of kinetic reactivity; at all potentials it is seen that the (100) surface has the slowest her kinetics, with an increase in rate on going to the (111) which is followed by a major increase in the current-density for the (110) face behaviour.
2. The shape of the curves; at low overpotentials, ca. $\eta > -70$ mV, a low Tafel slope, less than 60 mV decade^{-1}, is observed for all three planes. This is an indication of a potential dependence of the opd H coverage in that region. As the potential is increased an inflection is seen, the Tafel slope beyond this inflection achieving values greater than -120 mV decade^{-1} (2.303 $RT/\beta F$ for $\beta = 0.5$) which can be attributed to the chemical combination (Tafel) step becoming rate influencing, i.e. in this region the rates of the respective steps in the her mechanism are in the order: $v_2 < v_3 < v_1$, Fig. 5.

The potential range of this behaviour has a larger span for the Pt(100) and (111) planes than for the (110). After the potential is taken to even larger negative values a second inflection is seen. This is the transition from step III being rate-influencing to step II becoming rate-controlling[2] [18] which is inevitable due to the different potential dependences of steps II and III. The potential dependence of the rate of step III arises from the potential dependence of θ_{H} alone as opposed to step

[2] These types of inflections in the Tafel measurements have also been interpreted as resulting from the (actually unlikely) underpotential adsorption of the alkali metal ion (here Na^+). In the present study the proposed three-step her model represented the data extremely well so the process of metal ion underpotential deposition was not considered.

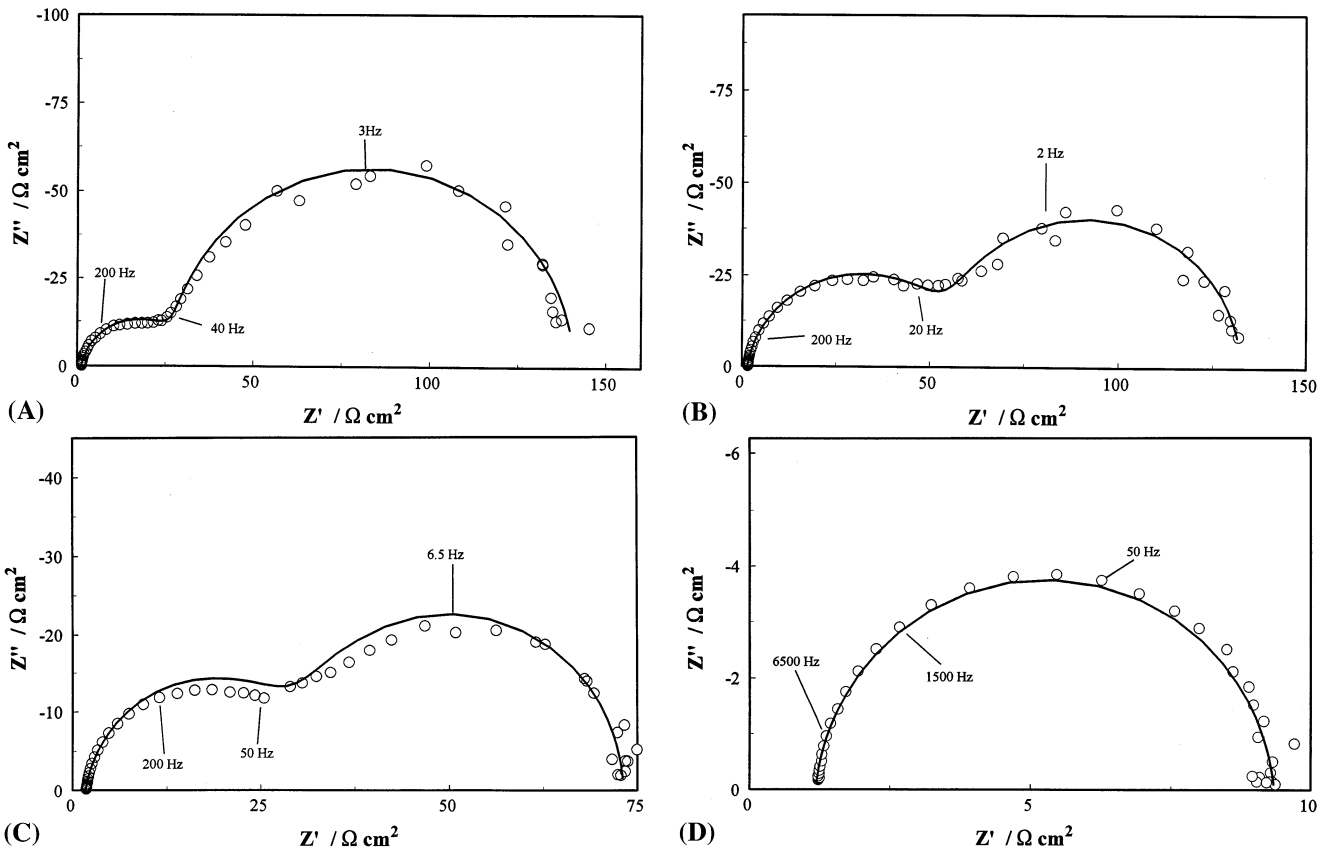

Fig. 6. Complex-plane plots of the EIS results for the (100) surface measured at four overpotentials; rotation rate 3000 rpm; frequency range covered 100 kHz to 0.1Hz. (A) −30 mV versus RHE; (B) −60 mV versus RHE; (C) −100 mV versus RHE and (D) −400 mV versus RHE.

II which has both the θ_H dependence and the Butler-Volmer charge-transfer term ($\exp(-\beta\eta F/RT)$) i.e. the potential is explicitly expressed in the rate equation for step II, (compare Eq. (2) and Eq. (3)). A summary of how each step behaves over the whole measured potential range is shown in Fig. 5 for the (100) face in relation to the total (j_{tot}) current-density. More in-depth descriptions and rigorous derivations of the potential dependence of the her and the opd H coverage as it relates to the 3-step her mechanism can be found in one of the many articles [16,17,19] or reviews on this topic [9,20–22].

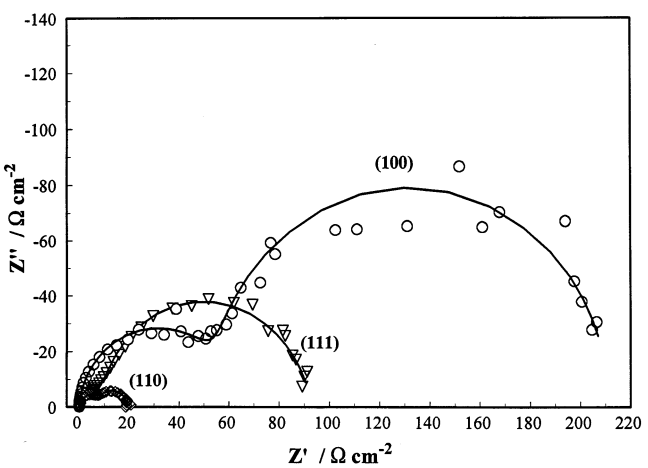

Fig. 7. A complex-plane plot comparing the EIS results for the three low-index planes at an overpotential of -40 ± 2 mV versus RHE. Frequency range 100 kHz to 0.1 Hz; rotation rate 3000 rpm; identification of Miller-indices is given on the plots; ○ (100), ▽ (111) and ◇ (110), open symbols are used in this plot for clarity.

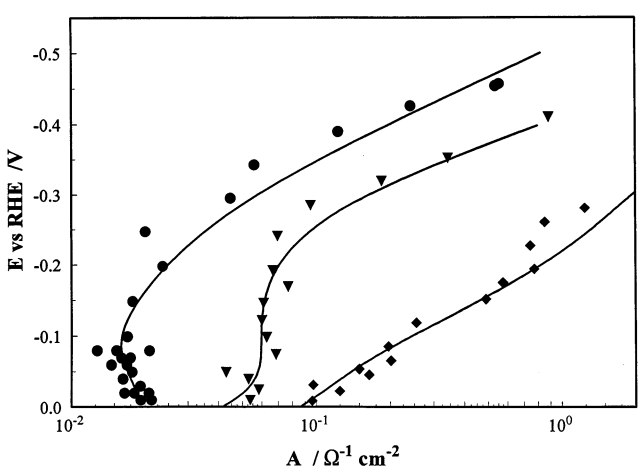

Fig. 8. A semilogarithmic plot of A (R_{ct}^{-1}) versus potential for the her at the three low-index planes of Pt. Rotation rate 3000 rpm; best fit line calculated from the rate constants in Table 1; ● (100), ▼ (111) and ◆ (110).

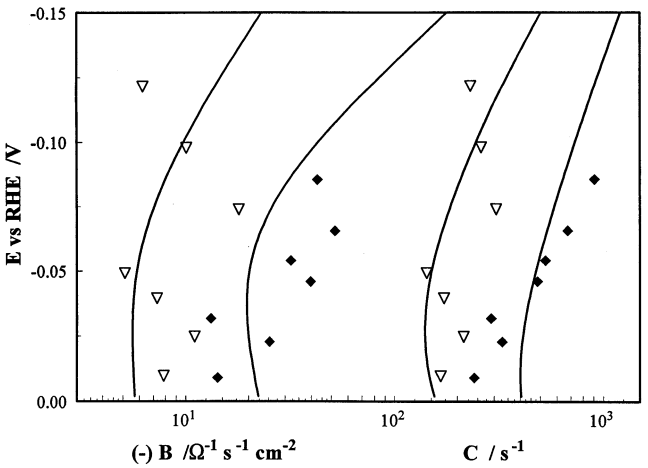

Fig. 9. A plot of the ac parameters $(-)B$ and C versus overpotential for the (111) and (110) surfaces. The best-fit lines were calculated from the rate-constants and q_1 given in Table 1. Note that the parameters B and C correspond to the second semicircle in the EIS complex-plane plots and that this process was resolved only at lower overpotentials ($\eta = 0$ to -100 mV); ▽ (111) and ◆ (110) open and closed symbols are used here to differentiate the two data sets.

Representative complex-plane plots showing the impedance data for the (100) face and the best fit curves to Eq. (7) are shown in Fig. 6(a, b, c, d). The results for the other faces, Pt(111) and (110), showed features similar to those seen for Pt (100) in Fig. 6 yet the magnitudes were different. The impedance spectra for all of the single-crystal surfaces studied consisted of the following components: (i) a higher-frequency process, which is assigned to electron transfer relaxing through the double-layer capacitance and (ii) a lower-frequency component associated with the modulation of the opd H coverage, θ_H, with the oscillation of potential. At low overpotentials, both dispersion processes are resolved

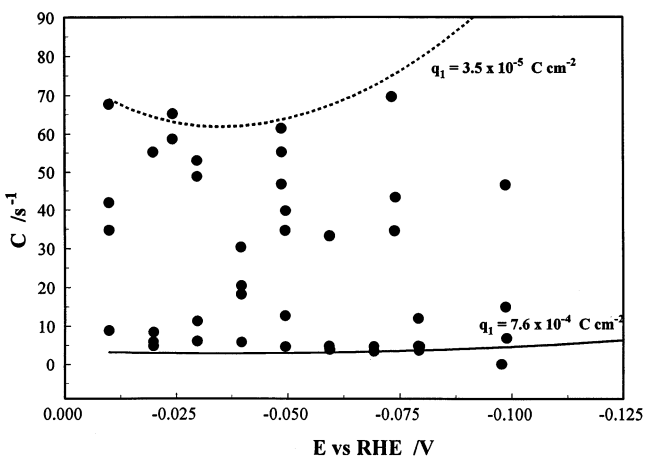

Fig. 10. A plot of C versus overpotential for the (100) surface, illustrating the degree of scatter that arises. The lines on the plot indicate the range of q_1 values which the scatter encompasses.

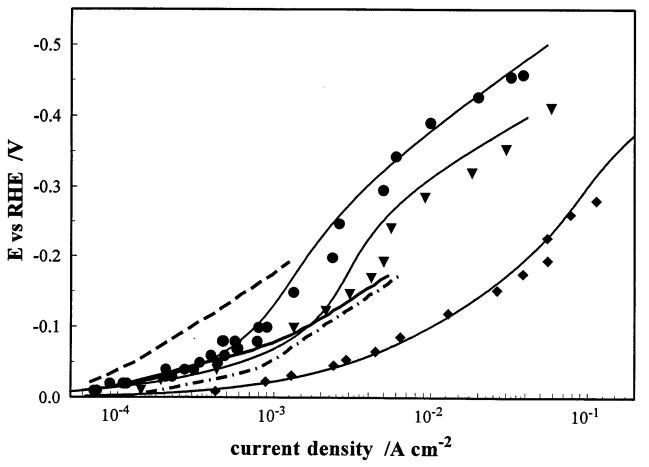

Fig. 11. A Tafel plot as in Fig. 4 but with the addition of the results from Marković et al. [23]; ● (100), ▼ (111) and ◆ (110) (the present data set); ---(111),—(100) and -·-(110) from Marković et al. [23].

(Fig. 6(a, b, c)) and at higher overpotentials (surface dependent) only the high-frequency process is seen (Fig. 6(d)). The decrease and eventual disappearance of the second dispersion process (the semicircle at higher real impedances (Z') on the complex-plane plot), indicates that, at higher overpotentials, the coverage of opd H is reaching a constant value; in the present case, its saturation limit, i.e. θ_H (opd) $\rightarrow 1$.

A comparison of the EIS data, plotted in the complex-plane, for the three low-index faces is given in Fig. 7 for a constant overpotential of approximately -40 mV. It should be noted that the charge-transfer resistance is smallest for the (110) face with a value of approximately 2 Ω cm^2 at $\eta = -150$ mV followed by a large increase in R_{ct} yielding, for the (111) face, a value of 16 Ω cm^2 with the (100) having the largest R_{ct} value which, at $\eta = -150$ mV, is 36 Ω cm^2, Fig. 8.

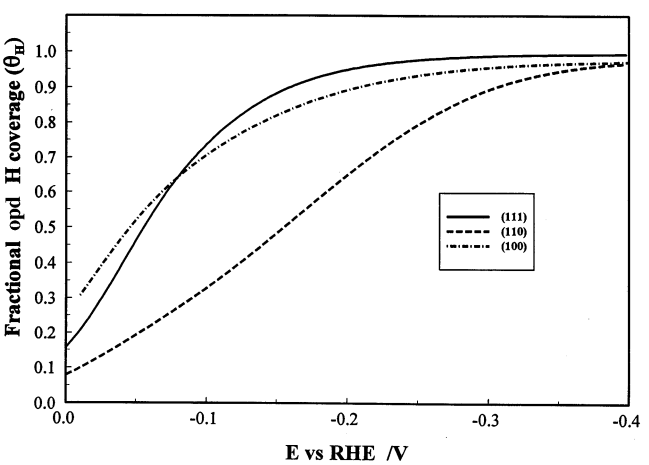

Fig. 12. A plot of fractional surface coverage of overpotentially deposited H as a function of overpotential for the three low-index planes. Note that to obtain the real surface H concentration the fractional coverage is to be multiplied by q_1; -·-(100),—(111) and ---(110).

Once the values of the constants (A, B and C) in Eq. (6) had been obtained from the CNLS fitting of the impedance data, the rate-constants and the q_1 value were obtained by a quantitative analysis of these values as a function of overpotential. The results of this analysis are shown in Figs. 8 and 9 for the A versus potential, and B and C versus potential relationships, the lines on these plots having been calculated from the best fit-rate constants and q_1 values shown in Table 1. For the (100) surface, as was noted in the experimental section, the current-density decreased significantly during the time needed to conduct the ac frequency scan. This did not lead to an unreasonable amount of scatter in the current–voltage or A versus potential relationships, but a large dispersion in the values for the parameters B and C did arise (Fig. 10). This problem of scatter was compounded by the fact that the fitting of either B or C led to substantially different q_1 values and that a value satisfying both parameters could not reliably be found. Many trials, studying the ac behaviour of this face, were performed in order to obtain consistent B and C versus potential relationships, but they were of no avail. Fig. 10 shows a plot of C versus potential illustrating the extent of the scatter. Also shown in Fig. 10 are the values of q_1 which encompass the limits of this scatter in C which gives an average q_1 value equal to $4\ (\pm 3) \times 10^{-4}$ C cm^{-2}, yielding a maximum opd H coverage between 0.17 and 3.6 apparent monolayers. The lower value seems more appropriate when compared to the value of 0.25 monolayers which was found in the work of Barber et al. [2] for acidic solutions, where the stability of the current-density was significantly better and much less scatter was observed in the relation of the ac parameters to potential pertaining to the opd H adsorption process.

Fig. 12 shows the calculated dependence of opd H coverage (θ_H) as a function of the electrode overpotential for the three low-index planes of Pt. The fractional opd H coverage at the reversible potential is related to the ratio of the rate-constants, i.e of the steps producing adsorbed H versus those in which it as a reactant, as in Eq. (5). From Fig. 12 it is seen that, at equilibrium, the order of opd H fractional coverage values is (100) > (111) > (110) but if one takes into account the concentration of active sites on the surface, which is measured by q_1, the absolute opd H coverage values become almost equivalent for the three faces, within the experimental error for the q_1 value.

The ratio of the rate constants for the steps in the her mechanism is also seen (Fig. 12) to influence the rate of change of θ_H with potential. The largest determining factor in this is the relative magnitudes of k_2 and k_3 in comparison with k_1. The sharper rise of θ_H for the (111) electrode compared with that for the (100) surface is mainly a result of the k_1/k_2 ratio being over three times greater for the (111) electrode (i.e. the production of θ_H is three times greater for the (111) surface relative to the (100) surface). The $\theta_H(\eta)$ curve for the (110) surface, on the other hand, has a much lower rate of change than that for either the (100) or the (111) surfaces due to the much greater activity of the Tafel step (k_3), relative to the Volmer step (k_{-1}) at the (110) surface. The ratio, k_1/k_3, is seen, from the values in Table 1, to be over an order of magnitude smaller for the (110) surface compared to that calculated for the (100) or (111) surfaces.

It can then be stated that not only does the overall rate depend on the Pt single-crystal surface geometry, but the distribution of the reaction affinity amongst the three steps is also surface sensitive.

5. Discussion of previous results

In order to assess the present data thoroughly and the conclusions drawn from it, it is necessary to discuss these findings in the light of previous work. It is unfortunate that, to our knowledge, only one other paper studying the her at Pt(hkl) surfaces in alkaline solutions has been published, viz. that of Marković et al. [23]. Upon comparison of the present results with those in Marković [23] (Fig. 11), it is readily noticed that the orders of electrocatalytic activity are different, i.e. in Marković et al. [23], (111) < (100) < (110) compared to the present results which show an order (100) < (111) < (110). The task therefore is to find a factor or factors which can account for this difference.

First of all there are differences in the two experimental procedures employed. The most significant difference is how the single-crystal face is isolated from the remainder of the electrode surface. In the present work the rotating meniscus (rm) technique was used whereas, in Marković et al. [23], a Teflon sleeve (ts) covered the sides of the crystal. Both techniques have advantages and disadvantages.

1. Using the rm method the preparation and installation of the electrode into the cell is simple and results can be obtained within seconds of the annealing/cleaning step whereas the ts procedure takes a longer time and much more manipulation of the electrode is required before it can be entered in a clean condition into the cell. This factor favours the rm method.
2. The isolation of the surface is guaranteed in the ts method (if no leakage occurs) whereas, as was stated in Barber et al. [2] using the rm method, the isolation of the desired surface is less assured and careful adjustment of the dimensions of the crystal, the meniscus and its positioning with regard to the Luggin capillary are important. For the face exhibiting the slowest kinetics a small kinetic influence from the sides was found in Barber et al., but this was minimised to a large degree by the above mentioned precautions [2]. This factor somewhat favours the ts method.

3. Providing a constant pressure of H_2 gas to the electrolyte is also a factor; in the ts method, H_2 can be bubbled continuously through the solution during measurements, whereas in the rm technique gas can be bubbled only before the crystal is placed in the cell and, after its installation, a constant pressure of H_2 is provided over the electrolyte. However, this did not seem to pose any problem and, if the H_2 flow was sufficiently large, a stable rest potential of 0.0 V versus RHE could be achieved using the rm method.

Tafel plots comparing the two sets of data are shown in Fig. 11 which clearly shows that the origin of the differences runs deeper than just the order of reactivity. In the present work the current-density covered is at least one decade more than that in Marković et al. [23]. This extra current and associated overpotential allows the transition between the rate-controlling processes to be seen, i.e. the Tafel to Heyrovsky (step II to step III) transition. Analysis of the data in [23], (linear Tafel plots which have a slope near 120 mV decade^{-1}), could falsely lead to a conclusion that the contribution from step III is negligible. For the (111) and (110) surfaces, the present results show greater activity than those from Marković et al. [23]. The only coincidence occurs at low overpotentials for the (100) surface and it is interesting that the current densities in Marković et al. [23] are larger at higher overpotentials for this plane.

Actually it was observed that if the (100) electrode was cooled in air it gave similar behaviour to the results shown by Marković et al. [23] for the (100) plane. This difference in the cooling conditions for the (100) surface is also consistent with the observations in acidic solutions [2]. The coincidence of the two (100) curves (Fig. 11) is also surprising due to the fact that (as seen from the results obtained by the rm method in 0.5 M H_2SO_4) because the (100) face suffers the most from edge effects although, taking the necessary precautions, it could be minimized. If edge effects had been important, this would have increased the measured apparent current-densities to larger values (due to greater accessible area) and a discrepancy going in the opposite direction would have been observed for the two (100) curves.

The differences seen in Fig. 11 between the two (110) results may be a result of the activation effect that was observed at this face over the first minute or so of application of potential. Although we are unsure of exactly what this activation process is, it was felt that the correct Tafel behaviour is found after this activation process has become completed. The reasoning behind this conclusion stems from the following observations: (i) the Tafel behaviour after this activation process is identical with that of the polycrystalline surface (electrode sealed in a Teflon sleeve and immersed in solution, [23]) which is also consistent with the findings when the 0.5 M H_2SO_4 electrolyte was used [2] and (ii) the CV for the (110) surface, after this activation process has taken place does not indicate reconstruction, only a slight deactivation[3]. It was also essential to our ac impedance measurements that a stable current-density was achieved, as was the case after this activation process had gone to completion.

The only behaviour which is inexplicable is the difference between the two plots (here and in [23] for the (111) surfaces), which is unfortunate since this is the result that leads to the apparent difference in order of reactivities.

6. Conclusions

The results presented in this paper provide a clear indication that the kinetics of the her are dependent on the surface geometry of the low-index planes of Pt single-crystal electrodes. Consistency with the results of our previous work performed in acidic media is very good. In *both* instances the order of reactivity is (100) < (111) < (110).

From both steady-state Tafel type and ac impedance measurements it was found that all three steps in the reaction mechanism participate significantly and a transition from step III to step II as rate-influencing is clearly shown to arise at each surface. The rate-constants for each reaction step were determined with good accuracy and reasonable values of the charge required for full coverage of opd H, q_1, were obtained for the (111) and (110) surfaces. Using 210 μC cm^{-2} as our reference, it is found that 27% and 54% of the (111) and (110) surfaces are maximally, respectively covered with opd H. At the (100) surface, much scatter was observed in the impedance parameters (B and C) pertaining to the H adsorption process but a definite q_1 value could not be found. A comparison with the results found in Barber et al. [2] would indicate that the maximum fractional coverage of the surface is below 25%.

One issue that arises from this work is that a substantial difference between the present results and those published by Marković et al. [23] exists. It appears these discrepancies arise from differences in experimental technique. Discussion of this matter was presented, but some points still need resolution.

Lastly, the three single-crystal surfaces were found to behave quite differently upon application of cathodic overpotential, i.e. the current-density decreased or increased with time, depending on potential, for the (100) face; it remained approximately constant for the (111) face and increased significantly at all potentials for the

[3] It may be the case that reconstruction takes place over the her potential region and then is lifted when the potentials are brought back to the upd of H potential range.

(110) electrode surface. The reasons for these changes are as yet unknown but some ideas concerning this phenomenon were given. The use of high-purity solutions and preparation techniques [24] makes it unlikely that the deactivating effects are due to poisoning impurities. They were not observed in similarly prepared acid solutions in the work of Barber et al. [2].

References

[1] S. Morin, H. Dumont and B.E. Conway, J. Electroanal. Chem. 412 (1996) 39, see also S. Morin, PhD Thesis, University of Ottawa (1996).
[2] J. Barber, S. Morin, and B.E. Conway, J. Electroanal. Chem., (1997) accepted for publication.
[3] H. Kita, S. Ye, Y. Gao, J. Electroanal. Chem. 334 (1992) 351.
[4] K. Seto, A. Iannelli, B. Love, J. Lipkowski, J. Electroanal. Chem. 226 (1987) 351.
[5] I.I. Pyshnograeva, A.M. Skundin, Yu.B. Vasiliev, V.S. Bagotsky, Electrokhimiya 6 (1970) 142.
[6] S. Schuldiner, M. Rosen, D. Flin, J. Electrochem. Soc. 117 (1970) 1251.
[7] S. Trasatti, J. Eletroanal. Chem. 39 (1977) 183.
[8] B.E. Conway, J. O'M. Bockris, J. Chem. Phys. 26 (1957) 532.
[9] B.E. Conway, B.V. Tilak, Adv. Catalysis 38 (1992) 1.
[10] A. Kutscher, W. Vielstich, Electrochim. Acta 8 (1963) 985.
[11] W. Vielstich, Brennstoffelemente, English translation, Fuel cells: modern processes for the electrochemical production of energy, Wiley-Interscience, New York, 1970.
[12] D. Jahn, W. Vielstich, J. Electrochem. Soc. 109 (1962) 849.
[13] L. Bai, J. Electroanal. Chem. 355, 37; L. Bai and B.E. Conway, Electrochim. Acta 31 (1986) (1993) 1013.
[14] J. Clavilier, K. El Achi, M. Petit, A. Rodes, M.A. Zamakhchari, J. Electroanal. Chem. 295 (1990) 333.
[15] H. Kita, S. Ye, A. Aramata, N. Furuya, J. Electroanal. Chem. 295 (1990) 317.
[16] D.A. Harrington and B.E. Conway, Electrochim. Acta 32 (1987) 1703; L. Bai, D.A. Harrington and B.E. Conway, Electrochim. Acta 32 (1987) 1713.
[17] A. Lasia, in: B.E. Conway, G. Jerkiewicz (Eds.), Proceedings of the Symposium on Electrochemistry and Materials Science of Cathodic Hydrogen Adsorption and Absorption, vol. 94-21, The Electrochemical Society, NJ, 1994, p. 261.
[18] T. Yamazaki, M. Enyo, Electrochim. Acta 35 (1990) 523.
[19] J. O'M Bockris, H. Mauser, Can. J. Chem. 37 (1959) 475.
[20] B.E. Conway, Theory and Principles of Electrode Processes, Ronald Press, New York, 1964.
[21] J. O'M Bockris, A.K.N. Reddy, Modern Electrochemistry, vol. 2, Plenum, New York, 1970.
[22] M. Enyo, in: B.E. Conway, J.O'M Bockris, E. Yeager, S.U.M. Khan and R.E. White (Eds.) Comprehensive Treatise of Electrochemistry, vol. 7, Plenum, NewYork, (1983).
[23] N.M. Marković, S.T. Sarraf, H.A. Gasteiger, P. Ross Jr, J. Chem. Soc. Faraday Trans. 92 (1996) 3719.
[24] B.E. Conway, H. Angerstein-Kozlowska, W.B.A. Sharp, E. Criddle, Anal. Chem. 45 (1973) 1331.